

EXTENDED CALCULATIONS OF SPECTROSCOPIC DATA: ENERGY LEVELS, LIFETIMES AND TRANSITION RATES FOR O-LIKE IONS FROM Cr XVII TO Zn XXIII

K. WANG^{1,2}, P. JÖNSSON², J. EKMAN², G. GAIGALAS³, M. R. GODEFROID⁴,
R. SI⁵, Z.B. CHEN⁶, S. LI⁷, C.Y. CHEN⁵, AND J. YAN^{7,8,9}

¹Hebei Key Lab of Optic-electronic Information and Materials, The College of Physics Science and Technology, Hebei University, Baoding 071002, China

²Group for Materials Science and Applied Mathematics, Malmö University, SE-20506, Malmö, Sweden; per.jonsson@mah.se

³Institute of Theoretical Physics and Astronomy, Vilnius University, Saulėtekio av. 3, LT-10222, Vilnius, Lithuania

⁴Chimie Quantique et Photophysique, CP160/09, Université libre de Bruxelles, Av. F.D. Roosevelt 50, 1050 Brussels, Belgium

⁵Shanghai EBIT Lab, Institute of Modern Physics, Department of Nuclear Science and Technology, Fudan University, Shanghai 200433, China; chychen@fudan.edu.cn

⁶College of Science, National University of Defense Technology, Changsha 410073, China chenzb008@qq.com

⁷Institute of Applied Physics and Computational Mathematics, Beijing 100088, China; lishuangwuli@126.com

⁸Center for Applied Physics and Technology, Peking University, Beijing 100871, China

⁹Collaborative Innovation Center of IFSA (CICIFSA), Shanghai Jiao Tong University, Shanghai 200240, China

ABSTRACT

Employing two state-of-the-art methods, multiconfiguration Dirac–Hartree–Fock and second-order many-body perturbation theory, the excitation energies and lifetimes for the lowest 200 states of the $2s^2 2p^4$, $2s 2p^5$, $2p^6$, $2s^2 2p^3 3s$, $2s^2 2p^3 3p$, $2s^2 2p^3 3d$, $2s 2p^4 3s$, $2s 2p^4 3p$, and $2s 2p^4 3d$ configurations, and multipole (electric dipole (E1), magnetic dipole (M1), and electric quadrupole (E2)) transition rates, line strengths, and oscillator strengths among these states are calculated for each O-like ion from Cr XVII to Zn XXIII. Our two data sets are compared with the NIST and CHIANTI compiled values, and previous calculations. The data are accurate enough for identification and deblending of new emission lines from the sun and other astrophysical sources. The amount of data of high accuracy is significantly increased for the $n = 3$ states of several O-like ions of astrophysics interest, where experimental data are very scarce.

Keywords: atomic data - atomic processes

1. INTRODUCTION

There is a wealth of observations from missions such as Chandra, XMM-Newton and Hinode. These observations require theoretical studies to supply more extensive atomic data of high accuracy. Considering this, we have recently provided accurate atomic data for L-shell ions, including the beryllium, boron, carbon, nitrogen, fluorine, and neon isoelectronic sequences (Jönsson et al. 2013; Ekman et al. 2014; Wang et al. 2014, 2015, 2016a,b; Radžiūtė et al. 2015; Si et al. 2016). In this paper, systematic calculations for oxygen-like ions from Cr XVII to Zn XXIII are reported.

Spectra of O-like ions, including the ions of the iron period, have been observed in various kinds of astronomical objects such as the sun, distant stars, and the Milky Way (Fawcett et al. 1987; Feldman & Doschek 1991; Landi et al. 1997; Feldman et al. 1998; Feldman et al. 2000; Behar et al. 2001; Dere et al. 2001; Mewe et al. 2001; Kaastra et al.

2002; Curdt et al. 2004; Landi & Phillips 2005, 2006; Raassen & Pollock 2013), as well as in laboratory plasmas (Brown et al. 2002; Fournier et al. 2003; May et al. 2005; Chen et al. 2007; Träbert et al. 2014; Yang et al. 2016). By analyzing lines of the spectra, properties of the plasmas, such as elemental abundances, electron density and temperature, can be determined. The $n = 3 \rightarrow 2$ emission lines of Fe XIX from the accumulated Chandra High Energy Transmission Grating (HETG) observations of Capella, for instance, were used for temperature and density diagnostics of the corona of Capella (Canizares et al. 2000; Kotochigova et al. 2010). Ni lines have been identified in the solar X-ray spectra (Phillips et al. 1982), and in the central region of the Perseus cluster (Tamura et al. 2009), and offer additional information on the emission measure distribution and density.

Many calculations have been performed for O-like ions. Most of them targeted atomic data for low-lying states of the $(1s^2)2s^2 2p^4$, $2s 2p^5$, and $2p^6$ config-

urations (the $n = 2$ complex) (Baluja & Zeippen 1988a,b; Galavis et al. 1997; Vilkas et al. 1999; Zhang & Sampson 2002; Gu 2005a; Hu et al. 2011; Rynkun et al. 2013; Fontes & Zhang 2015).

Because of their wide applications for analyzing new observations of astrophysical sources, as well as for modeling and diagnosing a variety of plasmas, energy and transition data for higher-lying states of the $n \geq 3$ complexes are also eagerly needed (Phillips et al. 1982; Acton et al. 1985; Landi & Phillips 2005; Kotochigova et al. 2007, 2010; Raassen & Pollock 2013). Among the studies of the $n \geq 3$ states of Fe XIX we mention the calculations of Jonauskas et al. (2004) using the multiconfiguration Dirac-Hartree-Fock (MCDHF) method, the calculations of Landi & Gu (2006) using the standard relativistic configuration interaction (RCI) method, the AUTOSTRUCTURE calculations of Butler & Badnell (2008), and the relativistic Breit-Pauli calculations of Nahar (2011). MCDHF calculations for Ni XXI were performed by Fan et al. (2013) for the lowest 86 states of the $n \leq 3$ configurations using the GRASP89 code (Dyall et al. 1989), and by Aggarwal et al. (2014) for the lowest 200 states of the $n \leq 3$ configurations using the GRASP0 code (Grant et al. 1980). Using a configuration interaction Dirac-Fock and Dirac-Fock-Sturm method combined with second-order Brillouin-Wigner perturbation theory, Kotochigova et al. (2007, 2010) computed the wavelengths and oscillator strengths for the $2s^2 2p^3 3s, 3d \rightarrow 2s^2 2p^4$ and $2s 2p^4 3p \rightarrow 2s^2 2p^4$ emission lines in the wavelength range from 12 Å to 16 Å with high accuracy. Excitation energies of the $2l^6$ and $2l^5 3l'$ states for Fe XIX and Ni XXI, and wavelengths of the $2l^5 nl'$, $n \rightarrow 2$ (with $3 \leq n \leq 7$) transitions for the same ions were reported by Gu (2005b, 2007) using a combined RCI and many-body perturbation theory (MBPT) method.

Energy and transition data of the $n = 2$ states provided by Vilkas et al. (1999); Gu (2005a); Rynkun et al. (2013) are of high accuracy and can be used to identify observed spectral lines among the $n = 2$ states. The data sets of the $n \geq 3$ states reported by Gu (2005b, 2007); Kotochigova et al. (2007, 2010) are also of high accuracy. However, Gu (2005b, 2007) provided energy data for O-like Fe and Ni but not transition rates, and Kotochigova et al. (2007, 2010) only reported transition wavelengths and rates in the range from 12 Å to 16 Å in Fe XIX. In comparison, the calculations by Landi & Gu (2006), Butler & Badnell (2008), and Nahar (2011) are quite inaccurate because of limited configuration interaction effects, though they provide complete sets of data including transition rates. For example, the energy values of Landi & Gu (2006), Butler & Badnell (2008), and Nahar (2011) for Fe XIX

depart from the compiled values in the Atomic Spectra Database (ASD) of the National Institute of Standards and Technology (NIST) (Kramida et al. 2015, <http://physics.nist.gov/asd>), as well as the present calculated values, by up to 1.2 %, 1.1 %, and 2.9 %, respectively. These gaps are too large for identification and deblending of emission lines in collisionally ionized plasmas such as the solar corona.

The present work provides consistent data sets of energy structures and transition characteristics with high accuracy for O-like ions in the range of nuclear charges $24 \leq Z \leq 30$. Employing two state-of-the-art methods, the MCDHF and RCI method implemented in the latest version of the GRASP2K code (Jönsson et al. 2013), and a combined RCI and MBPT approach in the FAC package (Gu 2008), the excitation energies and lifetimes of the lowest 200 states for the $2s^2 2p^4$, $2s 2p^5$, $2p^6$, $2s^2 2p^3 3s$, $2s^2 2p^3 3p$, $2s^2 2p^3 3d$, $2s 2p^4 3s$, $2s 2p^4 3p$, and $2s 2p^4 3d$ configurations, and multipole transition rates (electric dipole (E1), magnetic dipole (M1), and electric quadrupole (E2)) among these states are calculated for each ion from Cr XVII to Zn XXIII. The data sets obtained by the two theoretical methods are in excellent agreement. Compared with previous studies of O-like ions, our calculations result in a significant extension of accurate energy and transition data for higher-lying states of the $n = 3$ configurations, which will greatly improve the assessment of blending for diagnostic lines of interest, and aid the analysis of new spectra from astrophysical sources.

2. THEORY AND CALCULATIONS

2.1. MCDHF

In relativistic theory an atomic state is described by a wave function, which is a solution to the wave equation based on the Dirac-Coulomb Hamiltonian. In the MCDHF method, the wave function $\Psi(\gamma P J M)$ for a state labeled $\gamma P J M$ with γ being the orbital occupancy and angular coupling tree quantum numbers, P the parity, J the total angular momentum quantum number, and M the total magnetic quantum number, is expanded over configuration state functions $|\gamma_r P J M\rangle$ (CSFs)

$$|\Psi(\gamma P J M)\rangle = \sum_{r=1}^{\text{NCSFs}} c_r |\gamma_r P J M\rangle. \quad (1)$$

The CSFs are antisymmetrized and symmetry-adapted many electron functions built from products of one-electron Dirac orbitals (Grant 2007). Based on the extended optimal level (EOL) scheme, the radial parts of the Dirac orbitals and the expansion coefficients of the targeted states are optimized to self-consistency by solving the MCDHF equations, which are derived using the variational approach. The Breit interaction and lead-

ing QED effects (vacuum polarization and self-energy) are included in subsequent RCI calculations, where the best expansion coefficients are determined for the frozen one-electron orbital set. Transition parameters such as transition rates A , line strengths S or weighted oscillator strengths gf between two states $\gamma P J M$ and $\gamma' P' J' M'$ are expressed in terms of the submatrix element of the transition operator

$$\langle \Psi(\gamma P J) \| \mathbf{T} \| \Psi(\gamma' P' J') \rangle = \sum_{r,s} c_r c'_s \langle \gamma_r P J \| \mathbf{T} \| \gamma'_s P' J' \rangle, \quad (2)$$

where \mathbf{T} is the transition operator (Cowan 1981). The evaluation of the matrix elements follows the prescription given in Olsen et al. (1995).

The MCDHF and RCI calculations for the O-like ions were based on a multireference single and double (MR-SD) process for generating CSF expansions and a systematic procedure for monitoring convergence of computed excitation energies and transition parameters (Froese Fischer et al. 2016; Jönsson et al. 2013; Ekman et al. 2014). The MR for the even states consisted of the $2s^2 2p^4$, $2p^6$, $2s^2 2p^3 3p$, $2s 2p^4 3s$, $2s 2p^4 3d$, $2p^5 3p$, $2s^2 2p^3 4p$, $2s^2 2p^3 4f$, $2s 2p^4 4s$, $2s 2p^4 4d$ configurations. The MR for the odd states consisted of the $2s 2p^5$, $2s^2 2p^3 3s$, $2s^2 2p^3 3d$, $2s 2p^4 3p$, $2p^5 3s$, $2p^5 3d$, $2s^2 2p^3 4s$, $2s^2 2p^3 4d$, $2s 2p^4 4p$, $2s 2p^4 4f$ configurations. The CSFs were obtained by allowing SD substitutions from the subshells of the configurations in the MR to an active set of orbitals that was extended to orbitals with quantum numbers up to $n = 8$ and $l = 6$. The substitutions were limited so that at most one substitution was allowed from the $1s^2$ core. For the even states there were 6 787 000 CSFs distributed over the different J symmetries whereas for the odd states there were 7 130 000 CSFs. The calculations were done by parity meaning that all the even parity states were determined together in one set of calculations and all odd parity states were determined together in another set of calculations. All calculations were performed with the GRASP2K code (Jönsson et al. 2007; Jönsson et al. 2013).

2.2. MBPT

A detailed description of the combined RCI and MBPT method can be found in Lindgren (1974); Safronova et al. (1996); Vilkas et al. (1999). Gu (2008) implemented this method in the FAC package, which has successfully been used to calculate atomic data of high accuracy (Gu 2005b, 2007; Wang et al. 2014, 2015, 2016a,b; Si et al. 2016). In this method, the Hilbert space of the system is divided into two subspaces, including a model space M and an orthogonal space N . By means of solving the eigenvalue problem of a non-Hermitian effective Hamiltonian in the space M , we

can get the true eigenvalues of the Dirac–Coulomb–Breit Hamiltonian. The configuration interaction effects in the M space is exactly considered, and the interaction of the spaces M and N is accounted for with the many-body perturbation theory up to the second order. In our calculations, we include all states of the $2s^2 2p^4$, $2s 2p^5$, $2p^6$, $2s^2 2p^3 3s$, $2s^2 2p^3 3p$, $2s^2 2p^3 3d$, $2s 2p^4 3s$, $2s 2p^4 3p$, and $2s 2p^4 3d$ configurations in the model space M . Through the SD virtual excitations of the states spanning the M space, all states are contained in the space N . The maximum n values for the single/double excitations are 200/65, respectively, while the maximum l value is 20. Just as for the MCDHF and RCI calculations, QED corrections are also included.

3. EVALUATION OF DATA

3.1. Energy Levels

The computed excitation energies for all the 200 states of the $2s^2 2p^4$, $2s 2p^5$, $2p^6$, $2s^2 2p^3 3s$, $2s^2 2p^3 3p$, $2s^2 2p^3 3d$, $2s 2p^4 3s$, $2s 2p^4 3p$, and $2s 2p^4 3d$ configurations with $Z = 24 - 30$ from our MCDHF/RCI and MBPT calculations are listed in Table 1. In relativistic calculations the wave functions for the states are given as expansions over jj -coupled CSFs. To provide the LSJ labeling system used in databases such as the NIST ASD (Kramida et al. 2015) and CHIANTI (Del Zanna et al. 2015; Dere et al. 1997), the wave functions are transformed from a jj -coupled CSF basis into a LSJ -coupled CSF basis using the methods developed by Gaigalas et al. (2004). For each state numbered by a key (#), the configuration and LSJ designation, the compiled values from the NIST ASD when available, the radiative lifetime estimated from the theoretical transition rates (see section 3.2) and the eigenvector composition (largest expansion coefficients) are also included in Table 1 for the seven ions considered.

Since in astrophysics iron is of most concern, energies for all the 200 states from our MCDHF/RCI and MBPT calculations in Fe XIX are compared with the compiled data from the NIST and CHIANTI databases in Table 2. The previous theoretical values involving both the $n = 2$ and $n = 3$ states provided by Landi & Phillips (2005), Butler & Badnell (2008) and Nahar (2011) are also included. Due to the use of the same method and code, the MBPT energy data reported by Gu (2005b, 2007) have a similar accuracy as our MBPT values, and they are therefore not listed in Table 2. Our MCDHF/RCI and MBPT excitation energies for Fe XIX are in very good agreement. Defining $\Delta E_i \equiv (E_{\text{MBPT}}^i - E_{\text{MCDHF/RCI}}^i)$ for each of the N energy levels that can be compared ($i = 1, \dots, N$), the average absolute difference between the two sets calculated from

$$\overline{\Delta E} = \frac{\sum_{i=1}^N \Delta E_i}{N}, \quad (3)$$

with the standard deviation

$$\sigma_1 = \sqrt{\frac{\sum_{i=1}^N (\Delta E_i - \overline{\Delta E})^2}{(N-1)}}, \quad (4)$$

is found to be $\overline{\Delta E} \pm \sigma_1 = -566 \pm 548 \text{ cm}^{-1}$. That corresponds to an average relative difference of $\overline{\Delta x} \pm \sigma_2 = -0.009\% \pm 0.016\%$, with

$$\overline{\Delta x} \equiv \frac{\sum_{i=1}^N \Delta x_i}{N} = \frac{\sum_{i=1}^N (E_{\text{MBPT}}^i / E_{\text{MCDHF/RCI}}^i - 1)}{N}, \quad (5)$$

and

$$\sigma_2 = \sqrt{\frac{\sum_{i=1}^N (\Delta x_i - \overline{\Delta x})^2}{(N-1)}}. \quad (6)$$

The maximum difference is -2496 cm^{-1} for state $\#183/2s2p^4(^2P)3p^1P_1$ corresponding to about -0.03% . The previous theoretical energies of [Landi & Gu \(2006\)](#), [Butler & Badnell \(2008\)](#) and [Nahar \(2011\)](#) depart from our MCDHF/RCI values with average differences of $-81 \pm 7\,681 \text{ cm}^{-1}$, $16\,380 \pm 5\,674 \text{ cm}^{-1}$, and $75\,509 \pm 29\,681 \text{ cm}^{-1}$, respectively. The largest deviations from our MCDHF/RCI values are, respectively, $25\,898 \text{ cm}^{-1}$ ($\#183/2p^6\ ^1S_0$), $30\,764 \text{ cm}^{-1}$ and $97\,145 \text{ cm}^{-1}$ ($\#200/2s2p^4(^2P)3d\ ^1D_2$).

Most of the compiled NIST and CHIANTI energies listed in Table 2 show a good agreement with the present two data sets, except for a few states where the deviations from our values are larger than $10\,000 \text{ cm}^{-1}$. Furthermore, although the NIST ASD and CHIANTI database are claimed to be critically evaluated, discrepancies occur for some states. For these states our calculated values show good agreement with the results from the NIST database, thus resolving the inconsistencies. For example, the NIST compiled values for $\#12/2s^22p^3(^4S)3s\ ^3S_1$ and $\#25/2s^22p^3(^2P)3s\ ^3P_2$ agree well with the present calculations, while the corresponding values from the CHIANTI database deviate from our results by over $10\,000 \text{ cm}^{-1}$. For these states the CHIANTI observations seem to be wrong or at least affected by large uncertainties. To provide some insight in the difficulties of getting reliable excitation energies we look at the $2s^22p^3(^4S)3s\ ^3S_1$ state in more detail. With the aid of the known energy of the $2s^22p^4\ ^3P_2$ state, the CHIANTI energy $6\,670\,224 \text{ cm}^{-1}$ for $\#12/2s^22p^3(^4S)3s\ ^3S_1$ is obtained using the wavelength 14.992 \AA of the observation $2s^22p^3(^4S)3s\ ^3S_1 - 2s^22p^4\ ^3P_2$. This CHIANTI wavelength provided by [Landi & Phillips \(2005\)](#),

is about 0.15% higher than the NIST, MCDHF/RCI, and MBPT values (14.966 \AA , 14.969 \AA , and 14.969 \AA), but is much closer to the NIST, MCDHF/RCI, and MBPT results (14.995 \AA , 14.997 \AA , and 14.997 \AA) for the $2s^22p^3(^2D)3s\ ^1D_2 - 2s^22p^4\ ^1D_2$ transition. [Landi & Phillips \(2005\)](#) also pointed out that the CHIANTI energy for $2s^22p^3(^4S)3s\ ^3S_1$ was derived from a blended line of the $2s^22p^3(^4S)3s\ ^3S_1 - 2s^22p^4\ ^3P_2$ and $2s^22p^3(^2D)3s\ ^1D_2 - 2s^22p^4\ ^1D_2$ transitions. That line blending in the spectral observations compiled by the CHIANTI database is most likely responsible for the large deviation with the present theoretical values.

Compiled values from the NIST ASD are also questionable for a few $n = 3$ states of Fe XIX. The values $6\,923\,000 \text{ cm}^{-1}$ for $\#21/2s^22p^3(^2P)3s\ ^3P_1$, $7\,450\,000 \text{ cm}^{-1}$ for $\#78/2s^22p^3(^2P)3d\ ^3F_3$, $7\,567\,000 \text{ cm}^{-1}$ for $\#86/2s^22p^3(^2P)3d\ ^3P_1$, $7\,554\,000 \text{ cm}^{-1}$ for $\#90/2s^22p^3(^2P)3d\ ^3D_2$, and $7\,606\,000 \text{ cm}^{-1}$ for $\#92/2s^22p^3(^2P)3d\ ^1P_1$ do not have obvious counterparts in the present MCDHF/RCI and MBPT calculations. All these level energies have been included in Table 3.

To further assess the accuracy of our calculated energies, a comparison between the present MCDHF/RCI and MBPT values is carried out along the sequence with $Z = 24 - 30$. The compiled values from the NIST ASD are also included in the comparison. Good agreement between the present MCDHF/RCI and MBPT data is obtained, and the absolute average differences with the standard deviations decrease from $-623 \pm 606 \text{ cm}^{-1}$ for Cr XVII to $-397 \pm 536 \text{ cm}^{-1}$ for Zn XXIII, corresponding to the average differences from $-0.012\% \pm 0.021\%$ to $-0.009\% \pm 0.016\%$. Looking more carefully at the differences between the present two energy sets, we can observe that they are large for the $2s2p^4(^2P)3p\ ^1P_1$ and $2s2p^4(^2P)3d\ ^1D_2$ states in the sequence, and that the maximum differences decrease from -2872 cm^{-1} and -2699 cm^{-1} for Cr XVII to -1580 cm^{-1} and -1830 cm^{-1} for Zn XXIII. These states have specific radial characteristics compared with all other states arising from the same $2s2p^43p$ and $2s2p^43d$ configurations. An EOL calculation, which weights all states by a statistical weight factor of $2J + 1$, is strongly dominated by these other states and therefore produces radial orbitals less suited to describe the 1P_1 and 1D_2 states.

For the states of the seven O-like ions considered in our work, the 149 compiled energies listed in the NIST ASD are all included in Table 1. The NIST compiled values agree well with the present calculations for a majority of the states. However, there are about 41 states for which the NIST compiled values differ from our MCDHF/RCI results by over 4000 cm^{-1} (0.05%). All these 41 values and their reference sources have been listed in Table 3. These NIST compiled results should be reevaluated and used with care. As an example, in

Figure 1 (a) we show the deviations of the NIST energies to the present MCDHF/RCI results for some states as a function of Z . The deviations between the MBPT and MCDHF/RCI values for the same states along the sequence are shown in Figure 1 (b). A few of the NIST compiled values depart from the MCDHF/RCI data by over than $10\,000\text{ cm}^{-1}$, while good agreement is obtained between the present two data sets. Moreover the differences of two data sets vary smoothly along the isoelectronic sequence. Therefore, these values compiled by the NIST ASD, which have been listed in Table 3, seem to be wrong or at least are affected by large errors.

3.2. Radiative Rates

In Table 4, transition wavelengths, transition rates A , weighted oscillator strengths gf , and line strengths S are reported for O-like ions from Cr XVII to Zn XXIII. Transition data in the length form for the present MCDHF/RCI and MBPT calculations are listed for the E1, M1, and E2 transitions connecting the present 200 levels with A values larger than a fraction 10^{-3} of the sum of the A values for the transitions from the upper level, i.e., radiative branching ratios (BRs) larger than 0.1 %.

Since the transition data for iron are of particular interest in astrophysics, we compare the present MCDHF/RCI and MBPT rates for Fe XIX with rates from the CHIANTI and NIST databases. In Figure 2(a) the percentage deviations from the MBPT and CHIANTI A values to the MCDHF/RCI rates for the transitions with BRs greater than 1 % are shown. Many CHIANTI values differ from the MCDHF/RCI rates by 10%-100%, whereas the MBPT values agree with the MCDHF/RCI calculations to within 10%. The average difference and standard deviation of the MBPT and MCDHF/RCI calculations is $-1\% \pm 2\%$. The corresponding result from the CHIANTI values to the MCDHF/RCI rates is $2\% \pm 15\%$. The results of the comparisons can be explained by the fact that the MBPT and MCDHF/RCI calculations consider more electron correlation effects than the CHIANTI values, which are reported by Landi & Gu (2006) using the standard RCI method. The CHIANTI values are considered to be less accurate compared with the present two data sets.

In Figure 2 (b), transition rates recommended by the NIST ASD and the corresponding MBPT rates are also compared with the MCDHF/RCI A values. The rates of the present calculations agree within 1 % for most of the transitions, whereas the NIST rates differ from the present calculations by 10 %-90 % for many transitions. For example, the MCDHF/RCI and MBPT rates for the $2s^2 2p^3(^2D)3s\ ^1D_2 - 2s^2 2p^4\ ^3P_1$ transition are $2.66 \times 10^{11}\text{ s}^{-1}$ and $2.64 \times 10^{11}\text{ s}^{-1}$, respectively, while the corresponding NIST value is about one order of mag-

nitude smaller ($2.7 \times 10^{10}\text{ s}^{-1}$).

The above analysis leads us to the conclusion that compared with the CHIANTI and NIST transition data, our MCDHF/RCI and MBPT transition data are more accurate. As seen in Figure 2, the CHIANTI and NIST values differ from the MCDHF/RCI and MBPT rates relatively significantly, even for many strong transitions. Using many A values with less accuracy, particularly for strong transitions, to perform line identification or plasma modeling in astrophysics, quite different or even wrong results may be obtained. We highly recommend that the present MCDHF/RCI and MBPT transition data are used to update the CHIANTI and NIST data sets.

To further estimate the uncertainty of our transition data, the line strengths from our MCDHF/RCI calculations ($S_{MCDHF/RCI}$) for the E1 transitions are compared with the present MBPT line strengths (S_{MBPT}) in Figure 3. Our two data sets agree within 10 % for most of the transitions. According to the uncertainty estimation method suggested by Kramida (2014) we have the following averaged uncertainties for the S values of E1 transitions in various ranges of the line strengths: 2 % for $S \geq 10^{-1}$; 4 % for $10^{-1} > S \geq 10^{-2}$; 6 % for $10^{-2} > S \geq 10^{-3}$; 11 % for $10^{-3} > S \geq 10^{-4}$; 22 % for $10^{-4} > S \geq 10^{-5}$; and 30 % for $10^{-5} > S \geq 10^{-6}$. Considering the contribution from the uncertainty of the wavelengths, about 11.1 % transitions included in Table 4 have A -value uncertainties of $\leq 3\%$ (categories $A^+ \leq 2\%$ and $A \leq 3\%$ in the terminology of the NIST ASD), 61.3 % have uncertainties of $\leq 7\%$ (category B^+), 2 % have uncertainties of $\leq 10\%$ (category B), 15.5 % have uncertainties of $\leq 18\%$ (category C^+), 7.3% have uncertainties of $\leq 25\%$ (category C), 2.5 % have uncertainties of $\leq 40\%$ (category D^+), and only 0.3 % have uncertainties of $> 40\%$ (categories D and E). The uncertainty estimates of A values for each transition are listed in the last column of Table 4.

Again, using the method suggested by Kramida (2014), the uncertainties of the A values for the M1 and E2 transitions have been estimated. They are listed in Table 4 for each transition with BRs larger than 0.1 %.

3.3. Lifetimes

Our MCDHF/RCI and MBPT lifetimes are reported in Table 1, including the contribution from all possible E1, M1, and E2 radiative rates from the corresponding states.

Lifetimes for the first excited state 3P_0 of the configuration $2s^2 2p^4$ are dominated by the E2 transition $2s^2 2p^4\ ^3P_0 - ^3P_2$. Lifetimes for the other states 3P_1 , 1D_2 , and 1S_0 of the first excited configuration are determined by the M1 transitions to the ground state 3P_2 or to the state 3P_1 . The E2 A values from the states $2s^2 2p^3 3p, 3d$

to the states $2s^22p^4$ are important and contribute to the lifetimes for 10-40 %. For the other states considered in the present calculations, lifetimes are mostly determined by the E1 transitions. The present MCDHF/RCI and MBPT lifetimes agree to within 5% for most states. The two sets of level lifetimes with large deviations mostly occur for the transitions with large cancellation effects. Even a slight difference in the calculations may lead to a relatively large deviations for transition rates in these cases. More detailed discussion on these effects can be found in our recent work (Si et al. 2016).

4. SUMMARY

Employing two state-of-the-art methods (MCDHF/RCI and MBPT), the excitation energies and lifetimes of the lowest 200 states for the $2s^22p^4$, $2s2p^5$, $2p^6$, $2s^22p^33s$, $2s^22p^33p$, $2s^22p^33d$, $2s2p^43s$, $2s2p^43p$, and $2s2p^43d$ configurations have been calculated for O-like ions from Cr XVII to Zn XXIII. Wavelengths, line strengths, transition rates, and oscillator strengths for the E1, M1, and E2 transitions with BRs larger than 0.1 % are also reported.

There is a very good agreement between our MCDHF/RCI and MBPT results, and the absolute average energy differences with the standard deviations decrease from $-623 \pm 606 \text{ cm}^{-1}$ for Cr XVII to $-397 \pm 536 \text{ cm}^{-1}$ for Zn XXIII, corresponding to the average differences from $-0.012\% \pm 0.021\%$ to $-0.009\% \pm 0.016\%$. Lifetimes agree to within 5% for most states. Observed values listed in Table 3 compiled by the NIST ASD seem to be wrong or at least are affected by large errors. The present calculations provide a consistent and accurate data set for line identification and modeling purposes, which can also be considered as a benchmark for other calculations.

We acknowledge the support from the National Natural Science Foundation of China (Grant No. 11674066, No. 21503066, No. 11504421, and No. 11474034) and the Project funded by the China Scholarship Council (Grant No. 201608130201). This work is also supported by the Chinese Association of Atomic and Molecular Data, Chinese National Fusion Project for ITER No. 2015GB117000, the Swedish research council under contract 2015-04842 and the Belgian F.R.S.-FNRS Fonds de la Recherche Scientifique under CDR J.0047.16. The authors (K.W. and S. L.) express their gratefully gratitude to the support from the visiting researcher program at the Fudan University.

SCIENTIFIC SOFTWARE PACKAGES

Scientific software packages including

Software: FAC (Gu 2008), GRASP2K (Jönsson et al. 2007; Jönsson et al. 2013) are used

in the present work. We thanks the authors of these codes for providing support and guidance in using their codes.

REFERENCES

- Acton, L. W., Bruner, M. E., Brown, W. A., et al. 1985, *ApJ*, 291, 865
- Aggarwal, S., Verma, N., Singh, A., et al. 2014, *CaJPh*, 92, 1285
- Baluja, K. L., & Zeippen, C. J. 1988a, *JPhB*, 21, 15
- . 1988b, *JPhB*, 21, 1455
- Behar, E., Cottam, J., & Kahn, S. M. 2001, *ApJ*, 548, 966
- Brown, G. V., Beiersdorfer, P., Liedahl, D. A., et al. 2002, *ApJS*, 140, 589
- Butler, K., & Badnell, N. R. 2008, *A&A*, 489, 1369
- Canizares, C. R., Huenemoerder, D. P., Davis, D. S., et al. 2000, *ApJL*, 539, L41
- Chen, H., Gu, M. F., Behar, E., et al. 2007, *ApJS*, 168, 319
- Cowan, R. D. 1981, *The Theory of Atomic Structure and Spectra* (Berkeley, CA: Univ. California Press), doi:10.1007/978-0-387-35069-1
- Curdt, W., Landi, E., & Feldman, U. 2004, *A&A*, 427, 1045
- Del Zanna, G., Dere, K. P., Young, P. R., Landi, E., & Mason, H. E. 2015, *A&A*, 582, A56
- Dere, K. P., Landi, E., Mason, H. E., Monsignori Fossi, B. C., & Young, P. R. 1997, *A&AS*, 125, 149
- Dere, K. P., Landi, E., Young, P. R., & Del Zanna, G. 2001, *ApJS*, 134, 331
- Dyall, K., Grant, I., Johnson, C., Parpia, F., & Plummer, E. 1989, *CoPhC*, 55, 425
- Ekman, J., Jönsson, P., Gustafsson, S., et al. 2014, *A&A*, 564, A24
- Fan, Q., Jiang, G., Cao, L., Wang, W., & Du, S. 2013, *EpJD*, 67, 255
- Fawcett, B. C., & Hayes, R. W. 1975, *Mon. Not. R. Astron. Soc.*, 170, 185
- Fawcett, B. C., Phillips, K. J. H., Jordan, C., & Lemen, J. R. 1987, *MNRAS*, 225, 1013
- Feldman, U., Curdt, W., Doschek, G. A., et al. 1998, *ApJ*, 503, 467
- Feldman, U., Curdt, W., Landi, E., & Wilhelm, K. 2000, *ApJ*, 544, 508
- Feldman, U., & Doschek, G. A. 1991, *ApJS*, 75, 925
- Fontes, C. J., & Zhang, H. L. 2015, *ADNDT*, 101, 143
- Fournier, K. B., Faenov, A. Y., Pikuz, T. A., et al. 2003, *JPhB*, 36, 3787
- Froese Fischer, C., Godefroid, M., Brage, T., Jönsson, P., & Gaigalas, G. 2016, *JPhB*, 49, 182004
- Gaigalas, G., Zalandauskas, T., & Fritzsche, S. 2004, *CoPhC*, 157, 239
- Galavis, M. E., Mendoza, C., & Zeippen, C. J. 1997, *A&AS*, 123, 159
- Gordon, H., Hobby, M. G., & Peacock, N. J. 1980, *Journal of Physics B Atomic Molecular Physics*, 13, 1985
- Grant, I., McKenzie, B., Norrington, P., Mayers, D., & Pyper, N. 1980, *CoPhC*, 21, 207
- Grant, I. P. 2007, *Relativistic Quantum Theory of Atoms and Molecules*, doi:10.1007/978-0-387-35069-1
- Gu, M. F. 2005a, *ADNDT*, 89, 267
- . 2005b, *ApJS*, 156, 105
- . 2007, *ApJS*, 169, 154
- . 2008, *CaJPh*, 86, 675
- Hu, F., Yang, J., Wang, C., et al. 2011, *Open Physics*, 9, 1228
- Jonauskas, V., Keenan, F. P., Foord, M. E., et al. 2004, *A&A*, 424, 363
- Jönsson, P., Gaigalas, G., Bieroń, J., Froese Fischer, C., & Grant, I. P. 2013, *CoPhC*, 184, 2197
- Jönsson, P., He, X., Froese Fischer, C., & Grant, I. 2007, *CoPhC*, 177, 597
- Jönsson, P., Ekman, J., Gustafsson, S., et al. 2013, *A&A*, 559, p. A100
- Kaastra, J. S., Steenbrugge, K. C., Raassen, A. J. J., et al. 2002, *A&A*, 386, 427
- Kotochigova, S., Kirby, K. P., & Tupitsyn, I. 2007, *PhRvA*, 76, 052513
- Kotochigova, S., Linnik, M., Kirby, K. P., & Brickhouse, N. S. 2010, *ApJS*, 186, 85
- Kramida, A. 2014, *ApJS*, 212, 11
- Kramida, A., Yu. Ralchenko, Reader, J., & and NIST ASD Team. 2015, *NIST Atomic Spectra Database* (ver. 5.3), [Online]. Available: <http://physics.nist.gov/asd> [2016, May 10]. National Institute of Standards and Technology, Gaithersburg, MD., ,
- Landi, E., & Gu, M. F. 2006, *ApJ*, 640, 1171
- Landi, E., Landini, M., & Del Zanna, G. 1997, *A&A*, 324, 1027
- Landi, E., & Phillips, K. J. H. 2005, *ApJS*, 160, 286
- . 2006, *ApJS*, 166, 421
- Lindgren, I. 1974, *JPhB*, 7, 2441
- May, M. J., Beiersdorfer, P., Dunn, J., et al. 2005, *ApJS*, 158, 230
- Mewe, R., Raassen, A. J. J., Drake, J. J., et al. 2001, *A&A*, 368, 888
- Nahar, S. N. 2011, *ADNDT*, 97, 403
- Olsen, J., Godefroid, M. R., Jönsson, P., Malmqvist, P. Å., & Froese Fischer, C. 1995, *Phys. Rev. E*, 52, 4499
- Phillips, K. J. H., Fawcett, B. C., Kent, B. J., et al. 1982, *ApJ*, 256, 774
- Raassen, A. J. J., & Pollock, A. M. T. 2013, *A&A*, 550, A55
- Radziūte, L., Ekman, J., Jönsson, P., & Gaigalas, G. 2015, *A&A*, 582, A61
- Rynkun, P., Jönsson, P., Gaigalas, G., & Froese Fischer, C. 2013, *A&A*, 557, A136
- Safronova, M. S., Johnson, W. R., & Safronova, U. I. 1996, *PhRvA*, 53, 4036
- Shirai, T., Sugar, J., Musgrove, A., & Wiese, W. L. 2000, *JPCRD*
- Si, R., Li, S., Guo, X. L., et al. 2016, *ApJS*, 227, 16
- Tamura, T., Maeda, Y., Mitsuda, K., et al. 2009, *ApJL*, 705, L62
- Träbert, E., Beiersdorfer, P., Brickhouse, N. S., & Golub, L. 2014, *ApJS*, 211, 14
- Vilkas, M. J., Ishikawa, Y., & Koc, K. 1999, *PhRvA*, 60, 2808
- Wang, K., Li, D. F., Liu, H. T., et al. 2014, *ApJS*, 215, 26
- Wang, K., Guo, X. L., Liu, H. T., et al. 2015, *ApJS*, 218, 16
- Wang, K., Si, R., Dang, W., et al. 2016a, *ApJS*, 223, 3
- Wang, K., Chen, Z. B., Si, R., et al. 2016b, *ApJS*, 226, 14
- Yang, Z. H., Du, S. B., Su, M. G., Chang, H. W., & Guo, Y. P. 2016, *AJ*, 152, 135
- Zhang, H. L., & Sampson, D. H. 2002, *ADNDT*, 82, 357

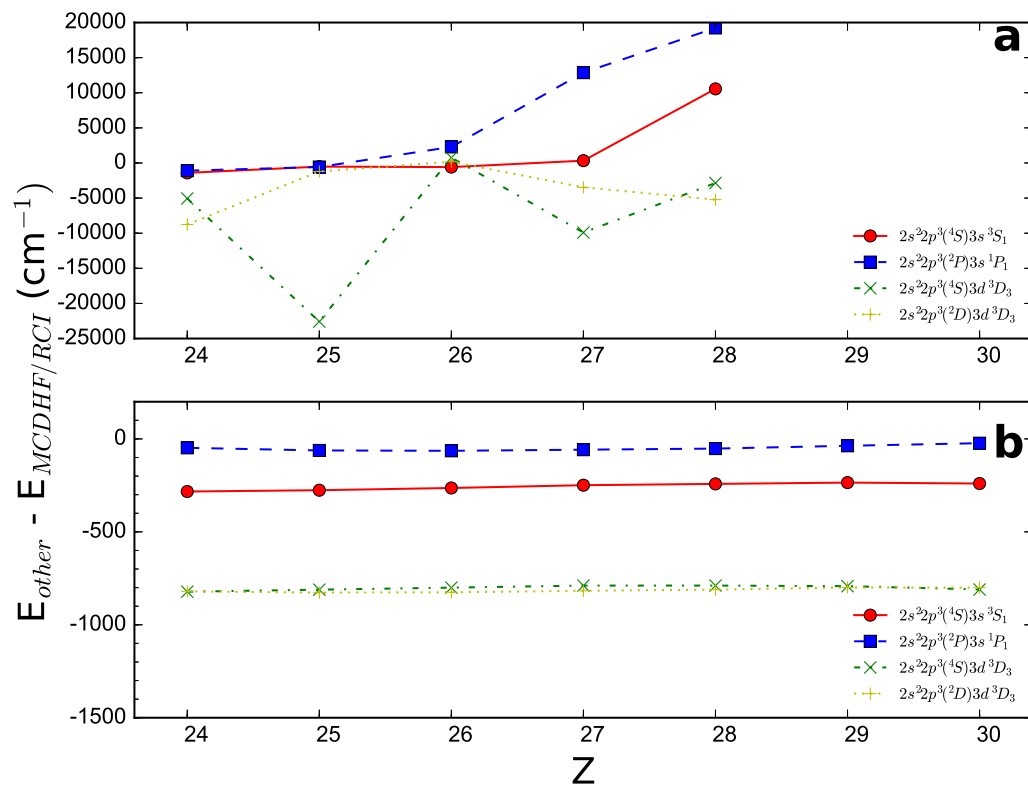


Figure 1. Energy deviations as a function of Z for some levels: (a) $E_{\text{NIST}} - E_{\text{MCDHF/RCI}}$ and (b) $E_{\text{MBPT}} - E_{\text{MCDHF/RCI}}$.

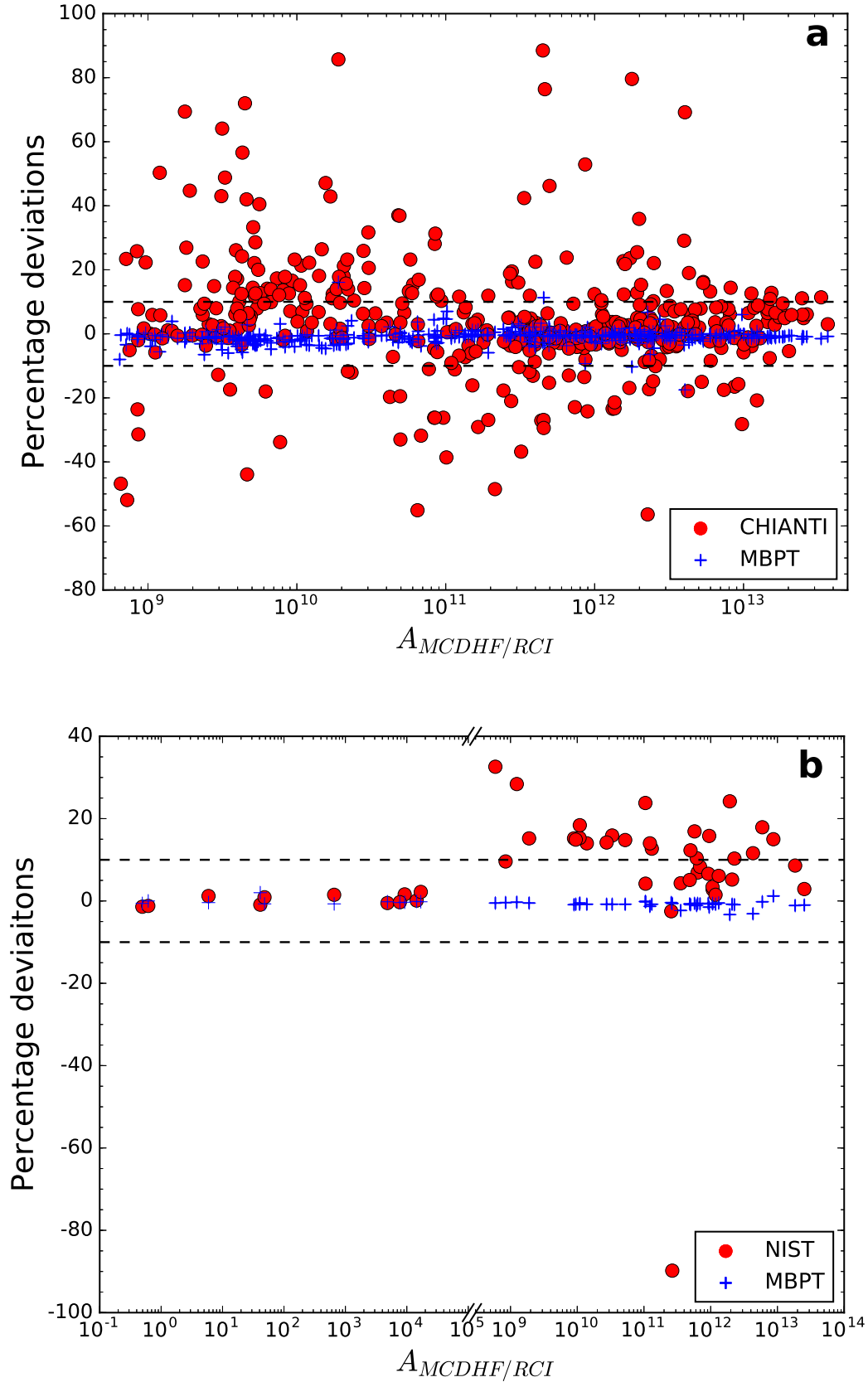


Figure 2. (a) Percentage deviations from the CHIANTI and MBPT rates to the MCDHF/RCI rates for the transitions with BRs greater than 1 % in Fe XIX. (b) Percentage deviations from the NIST and MBPT rates to the MCDHF/RCI rates for the transitions in Fe XIX listed by the NIST ASD. Dashed lines indicate the $\pm 10\%$ deviations.

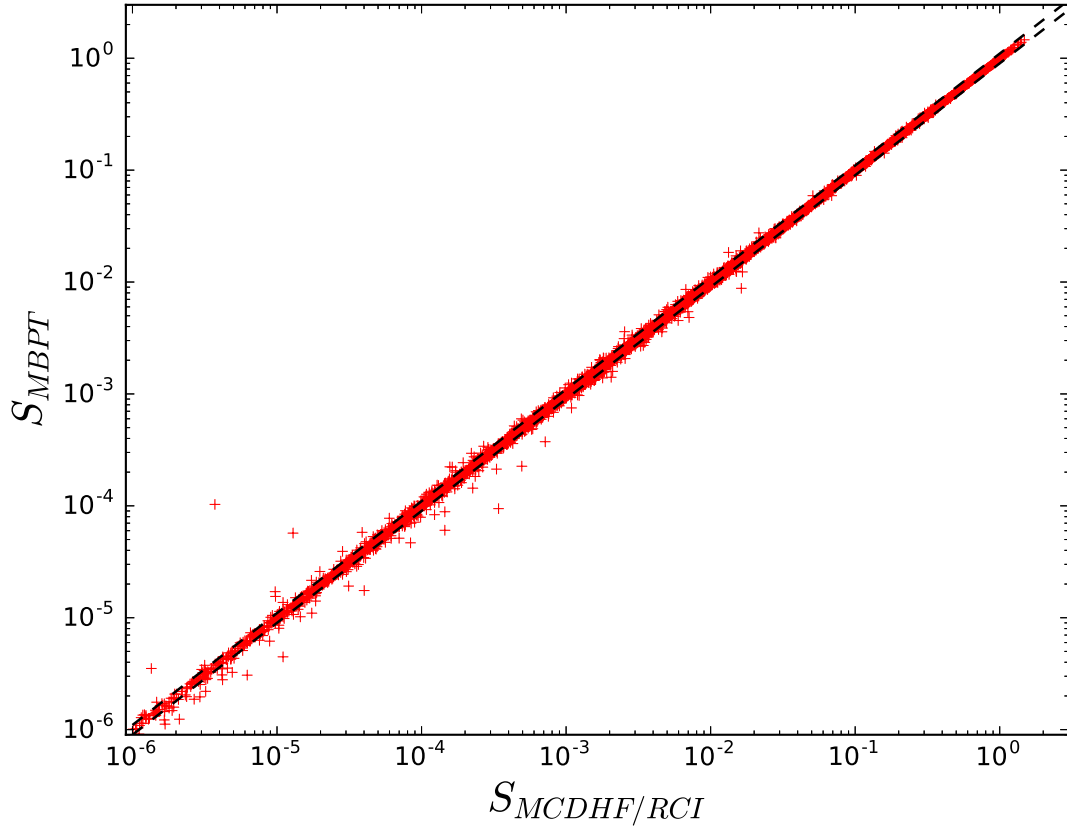


Figure 3. Comparison of the line strengths from our MCDHF/RCI ($S_{MCDHF/RCI}$) and MBPT (S_{MBPT}) calculations for the E1 transitions. Dashed lines indicate the $\pm 10\%$ deviations.

Table 1. Excitation energies (in cm^{-1}) and lifetimes (τ in s) for the lowest 200 levels of O-like ions with $Z = 24 - 30$. Subscripts MCDHF-/RCI and MBPT represent the theoretical values from our MCDHFR/RCI and MBPT calculations, respectively; subscript NIST represents the compiled values from the NIST ASD (Kramida et al. 2015). The rightmost column gives the LSJ coupling expansion coefficients of the states indicated by the keys in parenthesis.

Z	Key	Configuration	Term	E_{NIST}	$E_{\text{MCDHF/RCI}}$	E_{MBPT}	$\tau_{\text{MCDHF/RCI}}$	τ_{MBPT}	Coupling Expansion Coefficients
26	1	$2s^2 2p^4$	3P_2	0.000000E+00	0.000000E+00	0.000000E+00	0.95 (1) 0.31(4)
26	2	$2s^2 2p^4$	3P_0	7.525000E+04	7.532453E+04	7.525161E+04	2.032E+00	2.012E+00	0.89 (2) 0.44(5)
26	3	$2s^2 2p^4$	3P_1	8.944100E+04	8.943628E+04	8.953510E+04	6.887E-05	6.882E-05	-1.00 (3)
26	4	$2s^2 2p^4$	1D_2	1.688520E+05	1.689795E+05	1.688682E+05	5.696E-05	5.683E-05	0.95 (4) -0.31(1)
26	5	$2s^2 2p^4$	1S_0	3.251400E+05	3.254364E+05	3.252158E+05	7.176E-06	7.148E-06	-0.89 (5) 0.45(2)
26	6	$2s 2p^5$	3P_2	9.228900E+05	9.229189E+05	9.222972E+05	2.258E-11	2.242E-11	-1.00 (6)
26	7	$2s 2p^5$	3P_1	9.847400E+05	9.847962E+05	9.842101E+05	1.887E-11	1.875E-11	0.98 (7)
26	8	$2s 2p^5$	3P_0	1.030020E+06	1.030088E+06	1.029531E+06	1.910E-11	1.897E-11	1.00 (8)
26	9	$2s 2p^5$	1P_1	1.267600E+06	1.267989E+06	1.267227E+06	6.500E-12	6.458E-12	0.98 (9)
26	10	$2p^6$	1S_0	2.134180E+06	2.134803E+06	2.133030E+06	6.907E-12	6.844E-12	-0.99 (10)
26	11	$2s^2 2p^3 (4S) 3s$	5S_2	...	6.630146E+06	6.630311E+06	8.898E-12	8.857E-12	-0.95 (11)
26	12	$2s^2 2p^3 (4S) 3s$	3S_1	6.680000E+06	6.680585E+06	6.680321E+06	3.011E-13	2.988E-13	-0.91 (12)
26	13	$2s^2 2p^3 (2D) 3s$	3D_2	6.787000E+06	6.785245E+06	6.785219E+06	7.847E-13	7.807E-13	0.79 (13) -0.43(25) -0.35 (16)
26	14	$2s^2 2p^3 (2D) 3s$	3D_1	6.788000E+06	6.787272E+06	6.787176E+06	6.589E-13	6.544E-13	0.87 (14) 0.34(12)
26	15	$2s^2 2p^3 (2D) 3s$	3D_3	6.818000E+06	6.817623E+06	6.817516E+06	8.597E-13	8.550E-13	-1.00 (15)
26	16	$2s^2 2p^3 (2D) 3s$	1D_2	6.834000E+06	6.837049E+06	6.836843E+06	4.064E-13	4.033E-13	0.86 (16) 0.48(13)
26	17	$2s^2 2p^3 (4S) 3p$	5P_1	...	6.865440E+06	6.865468E+06	1.847E-10	1.817E-10	-0.94 (17)
26	18	$2s^2 2p^3 (4S) 3p$	5P_2	...	6.869100E+06	6.869117E+06	2.421E-10	2.389E-10	0.89 (18) 0.32(23)
26	19	$2s^2 2p^3 (4S) 3p$	5P_3	...	6.889411E+06	6.889494E+06	2.088E-10	2.056E-10	-0.95 (19)
26	20	$2s^2 2p^3 (2P) 3s$	3P_0	6.907000E+06	6.903083E+06	6.903147E+06	9.393E-13	9.345E-13	-0.99 (20)
26	21	$2s^2 2p^3 (2P) 3s$	3P_1	6.923000E+06	6.910492E+06	6.910590E+06	6.666E-13	6.628E-13	-0.87 (21) 0.47(26)
26	22	$2s^2 2p^3 (4S) 3p$	3P_1	...	6.918822E+06	6.918540E+06	1.183E-10	1.163E-10	-0.84 (22) -0.35(36) 0.34 (48)
26	23	$2s^2 2p^3 (4S) 3p$	3P_2	...	6.939924E+06	6.939562E+06	1.380E-10	1.355E-10	-0.82 (23) 0.41(18) -0.31 (37)
26	24	$2s^2 2p^3 (4S) 3p$	3P_0	...	6.949342E+06	6.948872E+06	1.285E-10	1.280E-10	0.93 (24)
26	25	$2s^2 2p^3 (2P) 3s$	3P_2	6.970000E+06	6.967324E+06	6.967410E+06	7.323E-13	7.273E-13	-0.84 (25) 0.36(16) -0.36 (13)
26	26	$2s^2 2p^3 (2P) 3s$	1P_1	6.985000E+06	6.982715E+06	6.982651E+06	4.259E-13	4.224E-13	-0.79 (26) -0.43(14) -0.36 (21)
26	27	$2s^2 2p^3 (2D) 3p$	3D_1	...	6.997089E+06	6.996933E+06	8.282E-11	8.145E-11	-0.69 (27) -0.58(31) 0.32 (22)
26	28	$2s^2 2p^3 (2D) 3p$	3F_2	...	7.018840E+06	7.018686E+06	2.036E-10	2.009E-10	-0.72 (28) 0.55(29) 0.34 (41)
26	29	$2s^2 2p^3 (2D) 3p$	3D_2	...	7.037578E+06	7.037457E+06	8.714E-11	8.622E-11	-0.77 (29) -0.52(28)
26	30	$2s^2 2p^3 (2D) 3p$	3F_3	...	7.040872E+06	7.040729E+06	1.960E-10	1.926E-10	-0.84 (30) 0.36(49) 0.35 (32)
26	31	$2s^2 2p^3 (2D) 3p$	1P_1	...	7.053002E+06	7.052839E+06	6.569E-11	6.496E-11	-0.69 (31) 0.61(27)
26	32	$2s^2 2p^3 (2D) 3p$	3D_3	...	7.053928E+06	7.053738E+06	6.801E-11	6.682E-11	0.73 (32) -0.63(33)
26	33	$2s^2 2p^3 (2D) 3p$	1F_3	...	7.074123E+06	7.073917E+06	1.605E-10	1.607E-10	0.68 (33) 0.59(32) 0.43 (30)
26	34	$2s^2 2p^3 (2D) 3p$	3F_4	...	7.079011E+06	7.078771E+06	1.862E-10	1.845E-10	-1.00 (34)
26	35	$2s^2 2p^3 (2D) 3p$	3P_0	...	7.096932E+06	7.096492E+06	1.429E-11	1.410E-11	-0.85 (35) -0.46(47)
26	36	$2s^2 2p^3 (2D) 3p$	3P_1	...	7.118296E+06	7.117799E+06	1.346E-11	1.330E-11	0.71 (36) -0.45(22) -0.43 (40) -0.32 (48)
26	37	$2s^2 2p^3 (2D) 3p$	3P_2	...	7.130871E+06	7.129782E+06	8.270E-12	8.094E-12	-0.85 (37) 0.37(23) 0.30 (54)
26	38	$2s^2 2p^3 (2P) 3p$	3D_1	...	7.143370E+06	7.143315E+06	3.165E-11	3.078E-11	-0.83 (38) -0.44(48)
26	39	$2s^2 2p^3 (2D) 3p$	1D_2	...	7.163798E+06	7.163254E+06	2.595E-11	2.581E-11	-0.77 (39) -0.42(54) 0.35 (55) -0.33 (37)
26	40	$2s^2 2p^3 (2P) 3p$	3S_1	...	7.174273E+06	7.174259E+06	2.148E-11	2.100E-11	-0.68 (40) -0.56(51) 0.37 (48) -0.31 (38)
26	41	$2s^2 2p^3 (2P) 3p$	3D_2	...	7.174461E+06	7.174449E+06	3.986E-11	3.866E-11	-0.89 (41)
26	42	$2s^2 2p^3 (4S) 3d$	5D_3	...	7.175573E+06	7.175245E+06	1.877E-11	1.846E-11	-0.94 (42)
26	43	$2s^2 2p^3 (4S) 3d$	5D_2	...	7.176083E+06	7.175746E+06	3.447E-12	3.426E-12	-0.95 (43)
26	44	$2s^2 2p^3 (4S) 3d$	5D_0	...	7.176619E+06	7.176227E+06	5.917E-12	5.902E-12	-0.95 (44)
26	45	$2s^2 2p^3 (4S) 3d$	5D_1	...	7.176850E+06	7.176505E+06	2.667E-12	2.661E-12	0.96 (45)
26	46	$2s^2 2p^3 (4S) 3d$	5D_4	...	7.178969E+06	7.178654E+06	2.171E-10	2.146E-10	-0.95 (46)

Table 1 continued

Table 1 (*continued*)

Z	Key	Configuration	Term	E_{NIST}	$E_{\text{MCDHF/RCI}}$	E_{MBPT}	$\tau_{\text{MCDHF/RCI}}$	τ_{MBPT}	Coupling	Expansion	Coefficients
26	200	$2s2p^4(^2P)3d$	1D_2	...	8.593096E+06	8.590723E+06	3.954E-14	3.873E-14	-0.77 (200)	-0.43(196)	0.35 (189) 0.32 (186)

NOTE— Table 1 is published in its entirety in the machine-readable format. The values for Fe XIX are shown here for guidance regarding its form and content.

Table 2. Energy levels (in cm^{-1}) relative to the ground state for the lowest 200 states of Fe XIX. For brevity, energies other than the present MCDHF values are listed as differences from the latter ones in cm^{-1} . $E_{\text{MCDHF/RCI}}$, E_{MBPT} -the present calculations; E_{NIST} -Kramida et al. (2015); $E_{\text{CHIANTI-Dere et al. (1997)}}$; Del Zanna et al. (2015); $E_{\text{Landi-Landi \& Gu (2006)}}$; $E_{\text{Butler-Butler \& Badnell (2008)}}$; $E_{\text{Nahar-Nahar (2011)}}$.

Key	Configuration	Term	E_{MCDHF}	E_{MBPT}	E_{NIST}	E_{CHIANTI}	E_{Landi}	E_{Butler}	E_{Nahar}
1	$2s^22p^4$	3P_2	0	0	0	0	0	0	0
2	$2s^22p^4$	3P_0	75325	-73	-75	-75	-126	-946	-45
3	$2s^22p^4$	3P_1	89436	99	5	5	-616	29	0
4	$2s^22p^4$	1D_2	168980	-111	-128	-128	1778	4810	-94
5	$2s^22p^4$	1S_0	325436	-221	-296	-296	-16	3186	-285
6	$2s2p^5$	3P_2	922919	-622	-29	-29	6312	8283	-28
7	$2s2p^5$	3P_1	984796	-586	-56	-56	6450	9451	-57
8	$2s2p^5$	3P_0	1030088	-557	-68	-68	5970	9665	-72
9	$2s2p^5$	1P_1	1267989	-762	-389	-389	14925	17065	-391
10	$2p^6$	1S_0	2134803	-1773	-623	-623	25898	29748	-621
11	$2s^22p^3(^4S)3s$	5S_2	6630146	165		714	-10051	13836	76187
12	$2s^22p^3(^4S)3s$	3S_1	6680585	-264	-585	-10361	-6295	16698	-589
13	$2s^22p^3(^2D)3s$	3D_2	6785245	-26	1755	-111	-8372	15836	1756
14	$2s^22p^3(^2D)3s$	3D_1	6787272	-96	728	-804	-7828	15844	727
15	$2s^22p^3(^2D)3s$	3D_3	6817623	-107	377	-526	-7623	19117	378
16	$2s^22p^3(^2D)3s$	1D_2	6837049	-206	-3049	2027	-6108	19818	-3048
17	$2s^22p^3(^4S)3p$	5P_1	6865440	28			-8430	13421	75654
18	$2s^22p^3(^4S)3p$	5P_2	6869100	17			-8215	13939	76273
19	$2s^22p^3(^4S)3p$	5P_3	6889411	83			-8097	12761	76198
20	$2s^22p^3(^2P)3s$	3P_0	6903083	64	3917		-13233	11031	3915
21	$2s^22p^3(^2P)3s$	3P_1	6910492	98	12508	-15786	-12583	11742	12506
22	$2s^22p^3(^4S)3p$	3P_1	6918822	-282			-6414	14675	77217
23	$2s^22p^3(^4S)3p$	3P_2	6939924	-362			-5676	15392	77031
24	$2s^22p^3(^4S)3p$	3P_0	6949342	-470			-5657	14514	77237
25	$2s^22p^3(^2P)3s$	3P_2	6967324	86	2676	-14672	-11058	12246	2675
26	$2s^22p^3(^2P)3s$	1P_1	6982715	-64	2285		-10193	12705	2285
27	$2s^22p^3(^2D)3p$	3D_1	6997089	-156			-7550	14790	78652
28	$2s^22p^3(^2D)3p$	3F_2	7018840	-154			-6789	16365	80275
29	$2s^22p^3(^2D)3p$	3D_2	7037578	-121			-6457	15234	80116
30	$2s^22p^3(^2D)3p$	3F_3	7040872	-143			-6537	16014	81179
31	$2s^22p^3(^2D)3p$	1P_1	7053002	-163			-7313	15605	81251
32	$2s^22p^3(^2D)3p$	3D_3	7053928	-190		-11087	-5680	17626	82630
33	$2s^22p^3(^2D)3p$	1F_3	7074123	-206		-6085	-5563	18376	83899
34	$2s^22p^3(^2D)3p$	3F_4	7079011	-240			-5652	18306	84323
35	$2s^22p^3(^2D)3p$	3P_0	7096932	-440			-4393	15759	78242

Table 2 *continued*

Table 2 (continued)

Key	Configuration	Term	E_{MCDHF}	E_{MBPT}	E_{NIST}	E_{CHIANTI}	E_{Landi}	E_{Butler}	E_{Nahar}
36	$2s^2 2p^3 ({}^2D)3p$	3P_1	7118296	-497			-5525	15500	80768
37	$2s^2 2p^3 ({}^2D)3p$	3P_2	7130871	-1089		-627	533	20164	83085
38	$2s^2 2p^3 ({}^2P)3p$	3D_1	7143370	-55			-9545	12931	81406
39	$2s^2 2p^3 ({}^2D)3p$	1D_2	7163798	-544			-4423	17111	82289
40	$2s^2 2p^3 ({}^2P)3p$	3S_1	7174273	-14			-10434	10688	80329
41	$2s^2 2p^3 ({}^2P)3p$	3D_2	7174461	-12			-9984	11802	81447
42	$2s^2 2p^3 ({}^4S)3d$	5D_3	7175573	-328		-942	-8158	14817	79194
43	$2s^2 2p^3 ({}^4S)3d$	5D_2	7176083	-337		-1452	-8191	13796	78245
44	$2s^2 2p^3 ({}^4S)3d$	5D_0	7176619	-392			-8348	12524	77116
45	$2s^2 2p^3 ({}^4S)3d$	5D_1	7176850	-345		-2219	-8246	13087	77643
46	$2s^2 2p^3 ({}^4S)3d$	5D_4	7178969	-315			-8228	15820	80275
47	$2s^2 2p^3 ({}^2P)3p$	3P_0	7213807	-935		10404	-3920	14642	83340
48	$2s^2 2p^3 ({}^2P)3p$	1P_1	7217770	-350			-7075	13046	83229
49	$2s^2 2p^3 ({}^2P)3p$	3D_3	7220791	-12			-9953	11309	82699
50	$2s^2 2p^3 ({}^4S)3d$	3D_2	7222063	-686		1428	-5303	18039	81076
51	$2s^2 2p^3 ({}^2P)3p$	3P_1	7243993	-366			-5566	13261	83025
52	$2s^2 2p^3 ({}^4S)3d$	3D_1	7247459	-853		3351	-3800	17992	80634
53	$2s^2 2p^3 ({}^4S)3d$	3D_3	7248240	-800	760	-1338	-4098	18541	766
54	$2s^2 2p^3 ({}^2P)3p$	3P_2	7252041	-112			-8998	11152	81517
55	$2s^2 2p^3 ({}^2P)3p$	1D_2	7272092	-1231			178	18545	86311
56	$2s^2 2p^3 ({}^2D)3d$	3F_2	7316663	-530		-3160	-6964	15605	53339
57	$2s^2 2p^3 ({}^2D)3d$	3F_3	7327947	-547		-866	-6549	17456	83733
58	$2s^2 2p^3 ({}^2D)3d$	1S_0	7329555	-549			-6121	16938	83277
59	$2s^2 2p^3 ({}^2D)3d$	3G_3	7334123	-629		-438	-5979	16862	82945
60	$2s^2 2p^3 ({}^2D)3d$	3G_4	7334980	-651			-6560	17958	84064
61	$2s^2 2p^3 ({}^2D)3d$	3D_1	7338653	-510		2983	-5670	16155	82531
62	$2s^2 2p^3 ({}^2D)3d$	3F_4	7357592	-502			-6194	19843	86889
63	$2s^2 2p^3 ({}^2D)3d$	3G_5	7369361	-759			-5832	21199	87838
64	$2s^2 2p^3 ({}^2D)3d$	1G_4	7369805	-884			-4635	20502	86922
65	$2s^2 2p^3 ({}^2P)3p$	1S_0	7373116	-1727			-491	17412	86695
66	$2s^2 2p^3 ({}^2D)3d$	3P_2	7377289	-667	-7289	157	-4278	17947	27708
67	$2s^2 2p^3 ({}^2D)3d$	1P_1	7384800	-583		-6904	-4622	18705	85436
68	$2s^2 2p^3 ({}^2D)3d$	3D_3	7395823	-825	177	-2046	-1483	22173	53179
69	$2s^2 2p^3 ({}^2D)3d$	3P_0	7400868	-723			-4155	19717	86399
70	$2s^2 2p^3 ({}^2D)3d$	3D_2	7403944	-733	1056	-55	-3267	19838	86100
71	$2s 2p^4 ({}^4P)3s$	5P_3	7402978	407			-5617	10705	79889
72	$2s^2 2p^3 ({}^2D)3d$	3P_1	7405460	-668		-1800	-3225	19877	86405
73	$2s^2 2p^3 ({}^2D)3d$	1D_2	7416210	-531			-6162	17642	51787
74	$2s^2 2p^3 ({}^2D)3d$	3S_1	7426777	-529		5001	-3557	19932	88660
75	$2s^2 2p^3 ({}^2D)3d$	1F_3	7447733	-1034	1267	-1541	-1010	22460	-51734
76	$2s 2p^4 ({}^4P)3s$	5P_2	7451737	194			-4922	10179	79305
77	$2s^2 2p^3 ({}^2P)3d$	3F_2	7464007	-412	3993		-9132	13519	83945
78	$2s^2 2p^3 ({}^2P)3d$	3F_3	7470689	-389	-20689	-13738	-9842	13708	-20688
79	$2s^2 2p^3 ({}^2P)3d$	1D_2	7484511	-566			-6305	16568	69488
80	$2s 2p^4 ({}^4P)3s$	5P_1	7486850	408			-5941	8438	78539
81	$2s^2 2p^3 ({}^2P)3d$	3D_1	7503198	-624		369	-6439	15171	63804
82	$2s 2p^4 ({}^4P)3s$	3P_2	7503423	-437		-5046	-1820	12295	79557
83	$2s^2 2p^3 ({}^2P)3d$	3F_4	7509040	-435			-9829	13992	86297
84	$2s^2 2p^3 ({}^2P)3d$	3P_0	7513823	-494			-7683	12600	84685

Table 2 continued

Table 2 (continued)

Key	Configuration	Term	E_{MCDHF}	E_{MBPT}	E_{NIST}	E_{CHIANTI}	E_{Landi}	E_{Butler}	E_{Nahar}
85	$2s^2 2p^3 ({}^2P) 3d$	3P_2	7524352	-363			-8418	14527	86392
86	$2s^2 2p^3 ({}^2P) 3d$	3P_1	7529372	-499	37628		-6631	14184	85498
87	$2s^2 2p^3 ({}^2P) 3d$	3D_3	7546342	-459		-1450	-7955	14471	18663
88	$2s 2p^4 ({}^4P) 3s$	3P_1	7554574	-621			-990	12073	79511
89	$2s^2 2p^3 ({}^2P) 3d$	1F_3	7564087	-1064	913		-1923	19052	86393
90	$2s^2 2p^3 ({}^2P) 3d$	3D_2	7568027	-731	-14027		-3855	16271	86458
91	$2s 2p^4 ({}^4P) 3s$	3P_0	7574350	-743		-1995	-771	11977	79422
92	$2s^2 2p^3 ({}^2P) 3d$	1P_1	7625309	-1025	-19309		-1824	18381	-19306
93	$2s 2p^4 ({}^4P) 3p$	5P_3	7635741	414		3095	-5689	8945	82205
94	$2s 2p^4 ({}^4P) 3p$	5P_2	7636730	353		2106	-5491	8865	81611
95	$2s 2p^4 ({}^4P) 3p$	5D_4	7667881	287			-4317	9532	83261
96	$2s 2p^4 ({}^4P) 3p$	5P_1	7678996	402			-5534	7241	81451
97	$2s 2p^4 ({}^4P) 3p$	3D_3	7680590	131		1082	-3456	10457	82952
98	$2s 2p^4 ({}^2D) 3s$	3D_1	7706931	-283			3941	18738	86086
99	$2s 2p^4 ({}^2D) 3s$	3D_2	7710256	-279		338	3932	19322	86877
100	$2s 2p^4 ({}^4P) 3p$	5D_2	7713092	173			-3858	9343	82340
101	$2s 2p^4 ({}^2D) 3s$	3D_3	7719690	-241			3340	20359	88932
102	$2s 2p^4 ({}^4P) 3p$	3S_1	7727129	24			-3315	9159	82448
103	$2s 2p^4 ({}^4P) 3p$	5D_0	7731488	217			-4478	7718	81216
104	$2s 2p^4 ({}^4P) 3p$	5D_1	7731674	134		5869	-2965	10144	82896
105	$2s 2p^4 ({}^4P) 3p$	5D_3	7736330	274		1213	-4606	7835	82322
106	$2s 2p^4 ({}^4P) 3p$	3P_2	7739205	-213		-1662	-2037	10725	83518
107	$2s 2p^4 ({}^4P) 3p$	5S_2	7762793	72			-3748	8094	82514
108	$2s 2p^4 ({}^2D) 3s$	1D_2	7769198	-899		-10199	6558	21657	87873
109	$2s 2p^4 ({}^4P) 3p$	3P_0	7777518	-370			-1363	11264	84502
110	$2s 2p^4 ({}^4P) 3p$	3D_1	7782230	-40			-2869	8632	82534
111	$2s 2p^4 ({}^4P) 3p$	3D_2	7784001	-186			-2135	10256	83331
112	$2s 2p^4 ({}^4P) 3p$	3P_1	7799644	-257			-1793	10444	83786
113	$2s 2p^4 ({}^2S) 3s$	3S_1	7860919	-308			1719	15635	85994
114	$2s 2p^4 ({}^2S) 3s$	1S_0	7892927	-787			5852	18525	86413
115	$2s 2p^4 ({}^2P) 3s$	3P_2	7909299	-519			10766	24296	90321
116	$2s 2p^4 ({}^2P) 3s$	1P_1	7921658	-590			11167	24246	90428
117	$2s 2p^4 ({}^4P) 3d$	5D_4	7921554	126			-7040	10315	85330
118	$2s 2p^4 ({}^4P) 3d$	5D_3	7922027	163			-6973	9239	84309
119	$2s 2p^4 ({}^4P) 3d$	5D_2	7929364	160			-6868	8195	83369
120	$2s 2p^4 ({}^2D) 3p$	3F_2	7932854	-386			5243	18862	90008
121	$2s 2p^4 ({}^2D) 3p$	1P_1	7938316	-632			5713	18704	88475
122	$2s 2p^4 ({}^4P) 3d$	5D_1	7941377	146			-6663	7740	83033
123	$2s 2p^4 ({}^4P) 3d$	5F_5	7946117	-193			-6612	11150	86325
124	$2s 2p^4 ({}^2D) 3p$	3F_3	7947902	-372			4974	19607	91542
125	$2s 2p^4 ({}^4P) 3d$	5D_0	7960762	100			-6778	7441	82819
126	$2s 2p^4 ({}^2D) 3p$	3F_4	7969045	-357			4346	19423	92116
127	$2s 2p^4 ({}^2D) 3p$	1F_3	7971309	-453			5995	19481	91070
128	$2s 2p^4 ({}^4P) 3d$	5F_4	7976602	-297			-5122	10814	85513
129	$2s 2p^4 ({}^2D) 3p$	3D_2	7981484	-490			6145	18942	90486
130	$2s 2p^4 ({}^4P) 3d$	5P_1	7989858	53			-5887	8536	84537
131	$2s 2p^4 ({}^2D) 3p$	3D_1	7992285	-623			6043	19061	89791
132	$2s 2p^4 ({}^4P) 3d$	5F_3	8000663	-215			-5528	9085	84629
133	$2s 2p^4 ({}^2D) 3p$	3D_3	8001383	-434			5274	19537	92381

Table 2 continued

Table 2 (continued)

Key	Configuration	Term	E_{MCDHF}	E_{MBPT}	E_{NIST}	E_{CHIANTI}	E_{Landi}	E_{Butler}	E_{Nahar}
134	$2s2p^4(^2D)3p$	1D_2	8005296	-575			6317	20014	91397
135	$2s2p^4(^4P)3d$	5P_2	8006455	-51			-5555	8846	84883
136	$2s2p^4(^2P)3s$	3P_1	8009187	-449			8777	21373	90788
137	$2s2p^4(^2D)3p$	3P_1	8015561	-1096			7931	20877	89429
138	$2s2p^4(^2D)3p$	3P_2	8017361	-1206			8949	20951	91634
139	$2s2p^4(^2D)3p$	3P_0	8019275	-1253			8366	19634	86088
140	$2s2p^4(^4P)3d$	3F_4	8022855	-314		2827	-4249	11517	85822
141	$2s2p^4(^2P)3s$	3P_0	8023208	-646			7250	19926	89979
142	$2s2p^4(^4P)3d$	5F_2	8023671	-98			-6579	7258	83832
143	$2s2p^4(^4P)3d$	5F_1	8027259	-187			-6673	6000	82800
144	$2s2p^4(^4P)3d$	5P_3	8032710	-132			-5098	10381	85909
145	$2s2p^4(^4P)3d$	3F_3	8043001	-209		1362	-3890	11337	85933
146	$2s2p^4(^4P)3d$	3P_0	8043463	-542			-109	14499	86250
147	$2s2p^4(^4P)3d$	3P_1	8047816	-468			-399	14209	86441
148	$2s2p^4(^4P)3d$	3D_2	8051510	-441			-1121	13413	86170
149	$2s2p^4(^4P)3d$	3F_2	8085548	-542		-360	-1627	12348	85701
150	$2s2p^4(^2S)3p$	3P_0	8090154	-712			4648	16977	89731
151	$2s2p^4(^4P)3d$	3D_1	8092034	-448			-668	13264	86403
152	$2s2p^4(^4P)3d$	3D_3	8098127	-532		-606	-335	13741	86949
153	$2s2p^4(^2S)3p$	3P_1	8099532	-579			5272	17597	89857
154	$2s2p^4(^4P)3d$	3P_2	8117304	-508		1630	-343	13576	86976
155	$2s2p^4(^2S)3p$	3P_2	8124923	-523			5268	16567	89453
156	$2s2p^4(^2S)3p$	1P_1	8134261	-743			5786	16673	89333
157	$2s2p^4(^2P)3p$	3P_2	8140136	-981			13298	24426	92917
158	$2s2p^4(^2P)3p$	1D_2	8161757	-804			13229	24147	93331
159	$2s2p^4(^2P)3p$	3D_3	8164737	-641			12784	23960	93709
160	$2s2p^4(^2P)3p$	3P_1	8174747	-1244			14057	24164	94322
161	$2s2p^4(^2P)3p$	1S_0	8192420	-1076			14391	24833	94613
162	$2s2p^4(^2P)3p$	3D_1	8215998	-769			12511	23502	94244
163	$2s2p^4(^2D)3d$	3G_3	8223512	-1186			3496	17900	90824
164	$2s2p^4(^2D)3d$	3G_4	8229906	-1178			3311	19581	92638
165	$2s2p^4(^2D)3d$	3G_5	8239680	-1173			2624	21196	94803
166	$2s2p^4(^2P)3p$	3P_0	8256103	-960			12784	22254	94391
167	$2s2p^4(^2D)3d$	3F_2	8260165	-1076			4795	18354	91306
168	$2s2p^4(^2P)3p$	3D_2	8263002	-605			10102	20844	93275
169	$2s2p^4(^2P)3p$	3S_1	8265578	-655			9949	20615	94134
170	$2s2p^4(^2D)3d$	3S_1	8267266	-611			3214	17878	92995
171	$2s2p^4(^2D)3d$	3F_3	8268206	-1041			4533	19885	93042
172	$2s2p^4(^2D)3d$	3F_4	8271994	-1084			4565	20894	94017
173	$2s2p^4(^2D)3d$	3D_1	8272556	-659			5163	19123	93894
174	$2s2p^4(^2D)3d$	3P_0	8273814	-1112			8976	22303	93799
175	$2s2p^4(^2D)3d$	3D_2	8280037	-1069			7704	22396	92865
176	$2s2p^4(^2D)3d$	1G_4	8286258	-1095			4851	22188	95292
177	$2s2p^4(^2D)3d$	3P_2	8286984	-1059			8415	23828	95257
178	$2s2p^4(^2D)3d$	3D_3	8287301	-1045			7032	23363	94150
179	$2s2p^4(^2D)3d$	3P_1	8292074	-1078			8603	22546	94041
180	$2s2p^4(^2D)3d$	1P_1	8313439	-1005			6017	21629	95391
181	$2s2p^4(^2D)3d$	1D_2	8314717	-1088			6794	22374	95002
182	$2s2p^4(^2D)3d$	1F_3	8318828	-1132			7937	23354	94622

Table 2 continued

Table 2 (continued)

Key	Configuration	Term	E_{MCDHF}	E_{MBPT}	E_{NIST}	E_{CHIANTI}	E_{Landi}	E_{Butler}	E_{Nahar}
183	$2s2p^4(^2P)3p$	1P_1	8326394	-2496			21922	29914	96219
184	$2s2p^4(^2D)3d$	1S_0	8334234	-1649			12097	27540	96412
185	$2s2p^4(^2S)3d$	3D_1	8396621	-1226			4237	16877	91769
186	$2s2p^4(^2S)3d$	3D_2	8403641	-1181			4097	17453	92343
187	$2s2p^4(^2S)3d$	3D_3	8407358	-1253			3587	18162	93158
188	$2s2p^4(^2P)3d$	3D_3	8428648	-1567		6826	11268	25158	95834
189	$2s2p^4(^2S)3d$	1D_2	8432474	-1512			7898	20923	93380
190	$2s2p^4(^2P)3d$	3D_2	8444387	-1604			11077	23901	94274
191	$2s2p^4(^2P)3d$	1F_3	8452605	-1853			13399	26053	95361
192	$2s2p^4(^2P)3d$	3F_4	8454188	-1694			12392	27153	96631
193	$2s2p^4(^2P)3d$	3P_1	8462101	-1695			12398	24357	94469
194	$2s2p^4(^2P)3d$	3P_0	8477203	-1775			14586	26113	94993
195	$2s2p^4(^2P)3d$	3D_1	8494763	-1752			13881	26381	96582
196	$2s2p^4(^2P)3d$	3F_2	8498362	-1920			14854	26892	95650
197	$2s2p^4(^2P)3d$	3F_3	8545614	-1539			10019	23618	96606
198	$2s2p^4(^2P)3d$	3P_2	8560908	-1385			9214	22333	96686
199	$2s2p^4(^2P)3d$	1P_1	8580920	-1745			15145	25832	96800
200	$2s2p^4(^2P)3d$	1D_2	8593096	-2373			19893	30764	97145

Table 3. Excitation energies (in cm^{-1}) for the states for which the NIST compiled values differ from our MCDHF/RCI values by more than 4000 cm^{-1} (0.05%), as well as their reference sources.

Z	Key ^a	Configuration	Term	Energy			ΔE		References
				MCDHF/RCI ^b	MBPT ^c	NIST ^d	MBPT&MCDHF/RCI	NIST&MCDHF/RCI	
24	54	$2s^2 2p^3(^4S)3d$	3D_3	5953561	5952739	5948500	-822	-5061	(Shirai et al. 2000)
24	68	$2s^2 2p^3(^2D)3d$	3D_3	6082766	6081946	6074000	-820	-8766	(Shirai et al. 2000)
24	75	$2s^2 2p^3(^2D)3d$	1F_3	6129342	6128282	6124400	-1060	-4942	(Shirai et al. 2000)
24	85	$2s^2 2p^3(^2P)3d$	3P_2	6181128	6180748	6131000	-380	-50128	(Fawcett & Hayes 1975; Shirai et al. 2000)
24	87	$2s^2 2p^3(^2P)3d$	3D_3	6199220	6198792	6164800	-428	-34420	(Fawcett & Hayes 1975; Shirai et al. 2000)
24	90	$2s^2 2p^3(^2P)3d$	3D_2	6218770	6218042	6214600	-728	-4170	(Fawcett & Hayes 1975; Shirai et al. 2000)
25	54	$2s^2 2p^3(^4S)3d$	3D_3	6585083	6584272	6562500	-811	-22583	(Fawcett & Hayes 1975; Shirai et al. 2000)
25	85	$2s^2 2p^3(^2P)3d$	3P_2	6835162	6834780	6778700	-382	-56462	(Fawcett & Hayes 1975; Shirai et al. 2000)
25	87	$2s^2 2p^3(^2P)3d$	3D_3	6855278	6854813	6803600	-465	-51678	(Fawcett & Hayes 1975; Shirai et al. 2000)
26	21	$2s^2 2p^3(^2P)3s$	3P_1	6910492	6910590	6923000	98	12508	(Gordon et al. 1980; Shirai et al. 2000)
26	66	$2s^2 2p^3(^2D)3d$	3P_2	7377289	7376622	7370000	-667	-7289	(Gordon et al. 1980; Shirai et al. 2000)
26	78	$2s^2 2p^3(^2P)3d$	3F_3	7470689	7470300	7450000	-389	-20689	(Gordon et al. 1980; Shirai et al. 2000)
26	86	$2s^2 2p^3(^2P)3d$	3P_1	7529372	7528873	7567000	-499	37628	(Gordon et al. 1980; Shirai et al. 2000)
26	90	$2s^2 2p^3(^2P)3d$	3D_2	7568027	7567296	7554000	-731	-14027	(Gordon et al. 1980; Shirai et al. 2000)
26	92	$2s^2 2p^3(^2P)3d$	1P_1	7625309	7624284	7606000	-1025	-19309	(Gordon et al. 1980; Shirai et al. 2000)
27	14	$2s^2 2p^3(^2D)3s$	3D_1	7453622	7453517	7447000	-105	-6622	(Gordon et al. 1980; Shirai et al. 2000)
27	20	$2s^2 2p^3(^2P)3s$	3P_0	7579349	7579398	7586000	49	6651	(Gordon et al. 1980; Shirai et al. 2000)
27	21	$2s^2 2p^3(^2P)3s$	3P_1	7587436	7587519	7599000	83	11564	(Shirai et al. 2000)
27	25	$2s^2 2p^3(^2P)3s$	3P_2	7659409	7659493	7668000	84	8591	(Gordon et al. 1980; Shirai et al. 2000)
27	27	$2s^2 2p^3(^2P)3s$	1P_1	7675137	7675079	7688000	-58	12863	(Gordon et al. 1980; Shirai et al. 2000)
27	52	$2s^2 2p^3(^4S)3d$	3D_3	7942904	7942115	7933000	-789	-9904	(Gordon et al. 1980; Shirai et al. 2000)
27	75	$2s^2 2p^3(^2D)3d$	1F_3	8156308	8155301	8150000	-1007	-6308	(Gordon et al. 1980; Shirai et al. 2000)
27	78	$2s^2 2p^3(^2P)3d$	3F_3	8183017	8182601	8157000	-416	-26017	(Gordon et al. 1980; Shirai et al. 2000)
27	79	$2s^2 2p^3(^2P)3d$	1D_2	8196128	8195542	8288000	-586	91872	(Gordon et al. 1980; Shirai et al. 2000)
27	85	$2s^2 2p^3(^2P)3d$	3P_2	8249180	8248832	8181000	-348	-68180	(Gordon et al. 1980; Shirai et al. 2000)
27	86	$2s^2 2p^3(^2P)3d$	3P_1	8253674	8253211	8237000	-463	-16674	(Gordon et al. 1980; Shirai et al. 2000)
27	90	$2s^2 2p^3(^2P)3d$	3D_2	8295397	8294685	8279000	-712	-16397	(Gordon et al. 1980; Shirai et al. 2000)
27	94	$2s^2 2p^3(^2P)3d$	1P_1	8356119	8355111	8331000	-1008	-25119	(Shirai et al. 2000)
28	12	$2s^2 2p^3(^4S)3s$	3S_1	8024448	8024206	8035000	-242	10552	(Gordon et al. 1980; Shirai et al. 2000)

Table 3 continued

Table 3 (continued)

Z	Key ^a	Configuration	Term	Energy			ΔE		References
				MCDHF/RCI ^b	MBPT ^c	NIST ^d	MBPT&MCDHF/RCI	NIST&MCDHF/RCI	
28	14	$2s^2 2p^3 ({}^2D) 3s$	3D_1	8152417	8152301	8146000	-116	-6417	(Gordon et al. 1980; Shirai et al. 2000)
28	20	$2s^2 2p^3 ({}^2P) 3s$	3P_0	8288106	8288139	8295000	33	6894	(Gordon et al. 1980; Shirai et al. 2000)
28	22	$2s^2 2p^3 ({}^2P) 3s$	3P_1	8296828	8296894	8313000	66	16172	(Shirai et al. 2000)
28	26	$2s^2 2p^3 ({}^2P) 3s$	3P_2	8386599	8386685	8405000	86	18401	(Gordon et al. 1980; Shirai et al. 2000)
28	27	$2s^2 2p^3 ({}^2P) 3s$	1P_1	8402772	8402720	8422000	-52	19228	(Gordon et al. 1980; Shirai et al. 2000)
28	68	$2s^2 2p^3 ({}^2D) 3d$	3D_3	8840222	8839411	8835000	-811	-5222	(Gordon et al. 1980; Shirai et al. 2000)
28	78	$2s^2 2p^3 ({}^2P) 3d$	3F_3	8928972	8928527	8895000	-445	-33972	(Gordon et al. 1980; Shirai et al. 2000)
28	79	$2s^2 2p^3 ({}^2P) 3d$	1D_2	8941104	8940501	9048000	-603	106896	(Gordon et al. 1980; Shirai et al. 2000)
28	85	$2s^2 2p^3 ({}^2P) 3d$	3P_2	9010165	9009830	8924000	-335	-86165	(Gordon et al. 1980; Shirai et al. 2000)
28	86	$2s^2 2p^3 ({}^2P) 3d$	3P_1	9014227	9013787	9000000	-440	-14227	(Gordon et al. 1980; Shirai et al. 2000)
28	91	$2s^2 2p^3 ({}^2P) 3d$	3D_2	9058604	9057909	9034000	-695	-24604	(Gordon et al. 1980; Shirai et al. 2000)
28	94	$2s^2 2p^3 ({}^2P) 3d$	1P_1	9123093	9122099	9090000	-994	-33093	(Shirai et al. 2000)

^a The index number of the level given in Table 1.

^b Our MCDHF/RCI energies.

^c Our MBPT energies.

^d The NIST recommended energies (Kramida et al. 2015).

Table 4. Transition data for O-like ions from Cr XVII to Zn XXIII. λ is transition wavelength in Å, S is line strength in atomic units, gf is weighted oscillator strength, and A is transition rate in s^{-1} . Only transitions which contribute to the total radiative lifetime by more than 0.1% are presented. The last column represents the estimated accuracies of the A -values using the terminologies of the NIST ASD (Kramida et al. 2015).

Z	j	i	Type	λ_{MCDHF}	λ_{MBPT}	S_{MCDHF}	gf_{MCDHF}	A_{MCDHF}	S_{MBPT}	gf_{MBPT}	A_{MBPT}	Acc.
24	2	1	E2	1.7207E+03	1.7194E+03	2.505E-03	8.276E-11	1.867E-01	2.486E-03	8.193E-11	1.846E-01	B+
24	3	1	M1	1.6541E+03	1.6562E+03	2.319E+00	5.662E-06	4.589E+03	2.308E+00	5.642E-06	4.585E+03	A
24	4	1	M1	7.4090E+02	7.4002E+02	4.890E-01	2.672E-06	6.509E+03	4.894E-01	2.671E-06	6.492E+03	A
24	4	3	M1	1.3420E+03	1.3378E+03	1.777E-01	5.371E-07	4.004E+02	1.779E-01	5.362E-07	3.972E+02	A
24	5	3	M1	4.9370E+02	4.9283E+02	2.602E-01	2.135E-06	5.864E+04	2.604E-01	2.133E-06	5.836E+04	A
24	6	1	E1	1.2307E+02	1.2295E+02	1.297E-01	3.205E-01	2.828E+10	1.289E-01	3.182E-01	2.803E+10	A+
24	6	3	E1	1.3296E+02	1.3281E+02	4.601E-02	1.052E-01	7.959E+09	4.576E-02	1.045E-01	7.888E+09	B+
24	6	4	E1	1.4758E+02	1.4745E+02	9.590E-03	1.976E-02	1.212E+09	9.586E-03	1.973E-02	1.208E+09	B+
24	7	1	E1	1.1668E+02	1.1658E+02	4.942E-02	1.288E-01	2.106E+10	4.914E-02	1.279E-01	2.090E+10	B+
24	7	2	E1	1.2516E+02	1.2506E+02	3.428E-02	8.327E-02	1.184E+10	3.407E-02	8.269E-02	1.174E+10	B+
24	7	3	E1	1.2553E+02	1.2541E+02	2.732E-02	6.616E-02	9.354E+09	2.716E-02	6.572E-02	9.273E+09	B+
24	7	5	E1	1.6833E+02	1.6821E+02	2.542E-03	4.591E-03	3.608E+08	2.541E-03	4.585E-03	3.598E+08	B+
24	8	3	E1	1.2099E+02	1.2087E+02	3.730E-02	9.373E-02	4.279E+10	3.708E-02	9.311E-02	4.243E+10	B+
24	9	1	E1	8.9641E+01	8.9564E+01	7.693E-03	2.609E-02	7.232E+09	7.686E-03	2.604E-02	7.206E+09	B+
24	9	2	E1	9.4568E+01	9.4486E+01	9.088E-04	2.922E-03	7.277E+08	9.123E-04	2.931E-03	7.286E+08	C+
24	9	3	E1	9.4777E+01	9.4684E+01	5.221E-04	1.675E-03	4.154E+08	5.209E-04	1.669E-03	4.132E+08	C+
24	9	4	E1	1.0198E+02	1.0190E+02	1.803E-01	5.375E-01	1.151E+11	1.792E-01	5.337E-01	1.141E+11	A+
24	9	5	E1	1.1730E+02	1.1720E+02	2.015E-02	5.222E-02	8.453E+09	2.006E-02	5.194E-02	8.394E+09	B+
24	10	7	E1	9.7275E+01	9.7148E+01	2.293E-03	7.170E-03	5.067E+09	2.285E-03	7.134E-03	5.029E+09	B+
24	10	9	E1	1.2995E+02	1.2976E+02	1.247E-01	2.919E-01	1.156E+11	1.238E-01	2.894E-01	1.143E+11	A+

Table 4 is published in its entirety in the machine-readable format. A portion is shown here for guidance regarding its form and content.